

## Study the Effect of New Rheocast on Tribological Behaviour of ZA27

Ali Kifah Ghazi<sup>a</sup> , Mohammed H. Abass<sup>b</sup>, Muhaed Alali<sup>c\*</sup> , Adnan N. Abood<sup>d</sup>

<sup>a</sup>Ministry of Higher Education and Scientific Research, Middle Technical University, Technical Engineering College-Baghdad, Baghdad, Iraq.

<sup>b</sup>Ministry of Oil, Midland Oil Company, Department of Engineering Inspection, Baghdad, Iraq.

<sup>c</sup>Ministry of Higher Education and Scientific Research, University of Kufa, Faculty of Engineering, Department of Materials Engineering, Najaf, Iraq.

<sup>d</sup>Middle Technical University, Baghdad, Iraq.

Received: December 05, 2022; Revised: March 12, 2023; Accepted: May 03, 2023

This paper investigated how casting affects ASTM ZA-27 alloy's tribological performance in dry and lubricated conditions. To this end, varying contact loads and sliding speeds were applied to tribological tests. The ZA-27 alloy was produced using gravity die casting (GDC) and new rheocasting (NRC) methods. The results showed that the microstructure of GDC ZA-27 alloy is dendritic containing  $\alpha$  and  $\eta$  phases. While the NRC alloy microstructure demonstrates a semi-globular structure of fine equiaxed  $\alpha$  phase bordered by eutectoid  $\alpha$  and  $\eta$ . The NRC alloy achieved an improvement in tensile, hardness, and elongation properties by almost 15%, 20%, and 25%, respectively. Regarding tribological properties, the NRC alloy achieved an enhancement in tribo-behavior by lowering the coefficient of friction (COF) to about 67% than the GDC alloy. Further, the results showed that the wear rate recorded an increment with applied load for both GDC and NRC alloys. Though, the results showed that the wear rate with NRC alloy was lower compared to the GDC alloy with about 84% at 160N normal load. The worn surfaces of NRC alloys were characterized by smooth and shallow wear grooves. While the GDC alloy worn surfaces were rougher and experience deeper grooves and damage.

**Keywords:** Gravity Die Casting, New Rheo-Casting, ZA-27, Tribological behavior.

### 1. Introduction

Improving tribomechanical systems is to date considered an essential objective that needs to be achieved in the industry, which can be performed from the aspect of rising friction and wear resistance. The typical way of achieving this objective is through the development and enhancement of tribological materials<sup>1,2</sup>. Zinc – Aluminum alloys (ZA alloys), is an attractive material for tribological applications, which is attracted essential attention from both researchers and industries during the last few years. Due to its significant castability and exceptional properties, commercial ZA alloys, particularly known as ZA-27, have become an important replacement material, primarily for aluminum cast alloys and bearing bronzes<sup>3,4</sup>. In particular, ZA-27 alloys can also compete with cast iron, plastics, and steel when used for service under heavy mechanical loads and low sliding speeds at normal service temperatures<sup>5</sup>. Besides, ZA-27 alloys are relatively inexpensive and can be easily manufactured with low energy consumption, without harming the environment<sup>6</sup>. Due to the aforementioned crucial advantages, ZA-27 alloys become an interesting subject for researchers. However, further modifications to the existing alloy standards are needed in order to develop a new enhanced version of the ZA-27<sup>7</sup>. To this end, one of the potential indicators for ZA alloy development is to improve its mechanical properties. This, for example, can be performed

by controlling the microstructure. Specifically, controlling the microstructure can be achieved by many techniques such as heat treatment and alloy casting type<sup>8</sup>. Improvement of mechanical and tribological properties of ZA-27 alloy can also be achieved by reinforcement with various forms of micro and nano-sized particles such as carbides (SiC, TiC)<sup>9,10</sup>, oxides ( $Al_2O_3$ ,  $Zn_2SiO_4$ , ZnO)<sup>11,12,13</sup>, and nanographene and graphite particles<sup>14,15</sup>. Another method to improve the alloy's performance, which is denoted by dimensional stability and creep resistance, is through the use of the rheo-casting technique<sup>16,17</sup>. This simple and flexible non-conventional casting method takes the advantage of the wide freezing range of ZA alloy to create a microstructure, which is consisting of degenerated dendrites immersed in a residual liquid and induced greater composition homogeneity<sup>18,19</sup>. The procedure of the conventional rheo-casting technique involves stirring the liquid metal by applying forces that are produced by electric, electromagnetic or ultrasonic fields while being cooled to certain temperatures between the liquid and solidus of the specific alloy and then cast. The obtained microstructure consists of a spherical primary solid microstructure. Rheocasting has significant advantages over conventional casting techniques, such as good net shape capability, low energy cost, less trapped air, and fine grain size<sup>20</sup>. However, recently a newly developed version of rheo-casting, termed new rheo-casting (NRC), is being produced. In the NRC method, cooling is controlled during

\*e-mail: [mowahid.alali@uokufa.edu.iq](mailto:mowahid.alali@uokufa.edu.iq)

**Table 1.** Chemical composition of ASTM ZA-27 alloy.

ASTM ZA-27 Alloy	Al%	Cu%	Mg%	Fe%	Cd%	Pb%	Zn%
Nominal chemical composition	25-28	2-2.5	0.01-0.02	0.1	0.003	0.004	Balance
ZA-27 Used	26.41	2.13	0.017	0.07	0.002	0.003	Balance
NRC alloy	26.38	2.10	0.016	0.071	0.002	0.003	Balance
GDC alloy	26.4	2.12	0.017	0.074	0.002	0.003	Balance

cast solidification to produce an equiaxed microstructure with a globular phase<sup>20,21</sup>. The NRC has the potential to enhance the compression strength, hardness, and elongation by rising the volume fraction of eutectic and refining the  $\alpha$ -Al phase grains in ZA-27 alloy. However, to date, there is a significant research challenge that needs to be addressed. Hence, investigating the effect of the casting method on the tribo-behavior of ZA-27 is required. Therefore, the attribution of this paper is to invest in the resulted microstructure of gravity die casting (GDC) and NRC methods to investigate their influence on the tribological behavior of ZA-27 alloy.

## 2. Experiment Work

### 2.1. Alloy preparation

ASTM ZA-27 alloy, with the chemical composition listed in Table 1, was used in this work. The ZA-27 alloy was casted in two methods, GDC and NRC. During the casting process, slag remover, (NaCl, KCl, NaF) was added to molten metal for protection from hydrogen as well as remove the oxides. For GDC, the molten alloy was degassed at 700°C, then cooled to 570°C and poured into a preheated (at 150°C) AISI H13 steel mold and lifted to solidify to obtain the ZA-27 blocks with the dimensions of (150×150×300) mm. Two K-type thermocouples with 1mm in diameter covered with stainless steel sheath were employed. The first thermocouple was used to measure the pouring temperature and the other was fixed in the mold wall through a hole to determine the cooling rate during solidification. For the NRC method, the molten ZA-27 was cooled to 530°C and then poured into a preheated AISI 304 stainless steel mold with dimensions of (60×60×120) mm. The pour was done through a 500 mm length fluid director. The director was made of a U-channel 304 stainless steel and inclined at 75° to boost the contact area between the molten metal and mold wall<sup>22,23</sup>. After that, it was backed with a copper strip to enhance the nucleation, which was achieved by increasing the heat dispersion. When the temperature reached 410°C, the stainless steel mold was quenched in agitated water. The steps of the NRC process are shown in Figure 1.

### 2.2. Microstructure and mechanical properties examinations

Microstructure examination was implemented using optical microscopy type MEIJI-Japan and scanning electron microscopy (SEM) type Thermo scientific Axia. The samples were prepared using standard grinding and polishing methods. Ground and polished samples were etched for 10sec in 5% $\text{HNO}_3$  + 95%Ethanol.

To evaluate the mechanical properties, the hardness of samples was measured by utilizing the Brinell hardness test

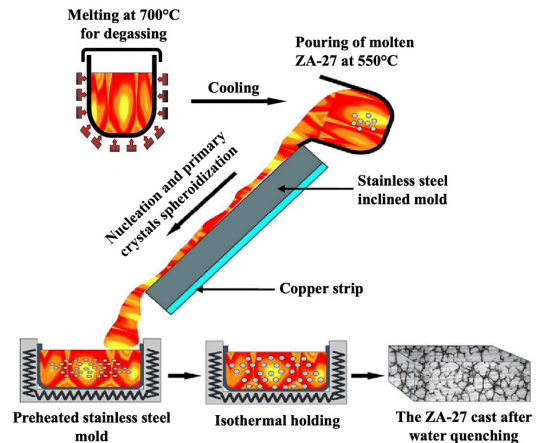


**Figure 1.** An illustration of steps with the NRC technique.

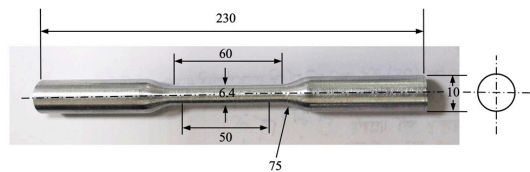


**Figure 2.** Tensile specimen according to the ASTM E8/E8M standard (All dimensions in mm).

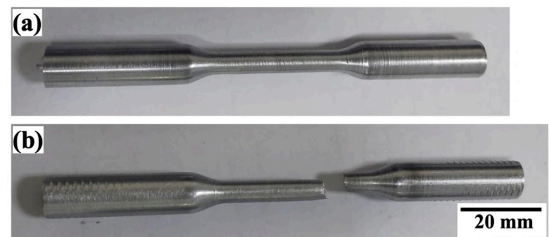


**Figure 3.** A tensile specimen (a) before the tensile test (b) after the tensile test

using a ball of 2.5 mm in diameter and a load of 31.25 kg. The tensile properties were evaluated using a universal tensile test machine type LARYEE. The tensile specimens were prepared according to the ASTM E8/E8M standard. The dimensions of the specimens (Figure 2) were specially designed for die-casting alloys. The tests were carried out at a 0.2mm/sec strain rate at room temperature. The tensile specimen before and after the tensile strength test are presented in Figure 3.

### 2.3. Friction and wear tests

Friction and wear tests were performed by utilizing a pin-on-disc Universal Friction and Wear Testing Machine. A schematic test-machine design is shown in Figure 4. Three rotating pins were put in contact with a fixed steel disc. The pins were prepared from ZA-27 alloy, which was produced by the GDC and NRC methods with dimensions of (4.3×4.3×15) mm and having a 5mm diameter spherical end. The disc with a diameter of 46.8 mm and 10 mm thick was made of alloy steel with a hardness of 63 HRC. The contact surfaces of the pins and disc were grounded and smoothed with SiC papers with up to 800 P. Friction tests were conducted under dry and lubricated conditions. The lubricant used was AA5W-30 commercial oil. The test was implemented for 900 sec for each sample and performed under a range of cycles and sliding speeds. The coefficient of friction (COF) was obtained automatically during the tests by employing the data analysis built-in software. Wear tests were performed under lubricated conditions. The wear behavior of pins was monitored, and the weight loss was calculated according to the ASTM G-99 standard. The tests were performed under various applied loads (20 – 160 N) with an increment of 20 N (the normal load was divided on the three pin specimens as shown in Figure 4). The test duration was 900 sec, the sliding speed was 1.7 m/sec, and every test was repeated three times. The SEM was used to examine the worn surfaces of the tested wear pins. During the lubricated condition of both friction and wear tests, the disc was continuously and completely immersed in 50 ml of lubricant.

### 2.4. Friction and wear calculation

The friction and wear calculate depending on ASTM G99-05 and ASTM G40-15 calculations.

The coefficient of friction for the three pins  $\mu = \frac{3f}{3P}$  (1)

So, the COF for one pin  $\mu = \frac{f}{P}$  (2)

Weight losses calculated by weighting the samples before and after testing  $\Delta w = w_2 - w_1$  (3)

To convert, the weight losses to volume losses divided  $\Delta w$  by the density of ZA27 alloy (5 g/cm<sup>3</sup>)

Volume losses  $V = \frac{\Delta w}{\rho} \times 1000$  (4)

The wear rate is the quantity of material removed in unit distance of sliding  $Wr = \frac{V}{SD}$  (5)

The hardness is an important factor that affects the wear rate, the relation between hardness and material losses explains by Archard's law:  $V = \frac{k P S D}{H}$  (6)

So that, Coefficient of wear  $k = \frac{V H}{P S D}$  (7)

Where:

$f$ : frictional load (N).

$P$ : Normal applied load (N).

$\mu$ : Coefficient of friction (unit less).

$\Delta w$ : weight losses (g).

$w_1$ : weight of samples before the test (g).

$w_2$ : weight of samples after the test (g).

$V$ : Volume losses (mm<sup>3</sup>).

$\rho$ : density (g/cm<sup>3</sup>).

$SD$ : sliding distance (m).

$Wr$ : Wear rate (mm<sup>3</sup>/m).

$H$ : hardness of soft material (kg/mm<sup>2</sup>).

$k$ : Coefficient of wear (unit less).

## 3. Results and Discussion

This section provides the experiment comparison results. This section presents several experimental results, which characterize the performance of ZA-27 alloys.

### 3.1. Microstructure and mechanical properties

The microstructure of ZA-27 alloy made with the GDC method exhibited a typical dendritic structure containing two phases ( $\alpha$  and  $\eta$ ) as shown in Figure 5. The light-colored cores that are rich in aluminum represent the  $\alpha$  phase, and between them is a grey-colored eutectic structure containing the  $\alpha$  phase and zinc-rich  $\eta$  phase<sup>24</sup>. For the ZA-27 alloy produced by the NRC technique, the microstructure demonstrated a

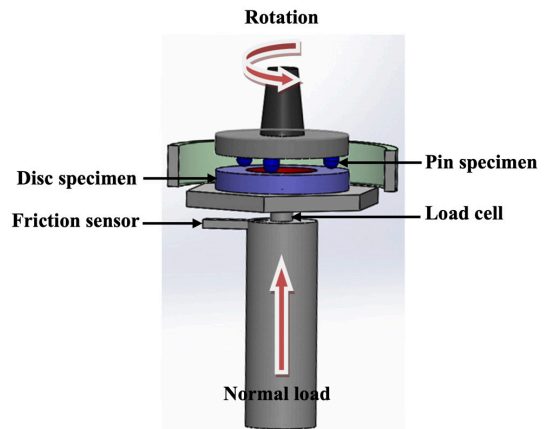


Figure 4. Schematic of friction and wear test machine.

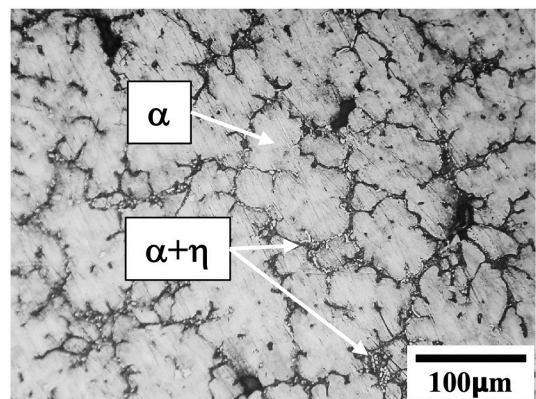
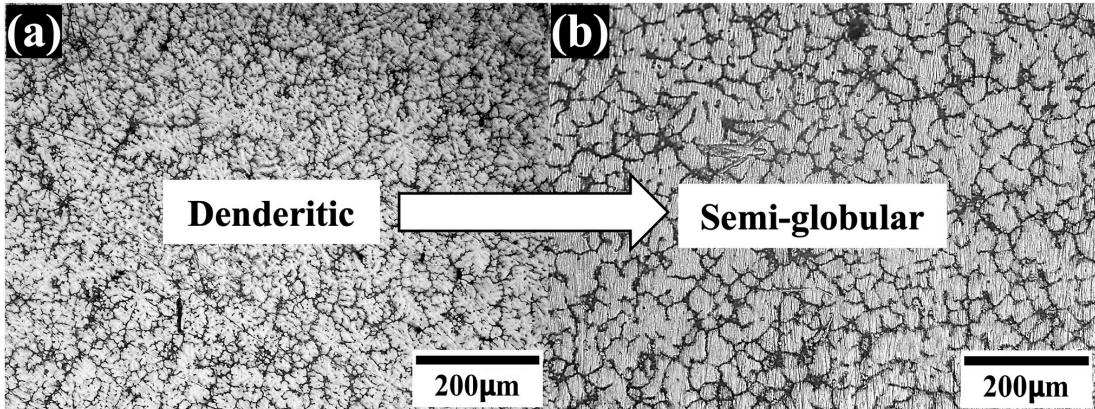


Figure 5. Microstructure of the ZA-27 alloy produced by GDC.

**Table 2.** Mechanical properties of ZA-27 alloys produced with GDC and NRC methods.

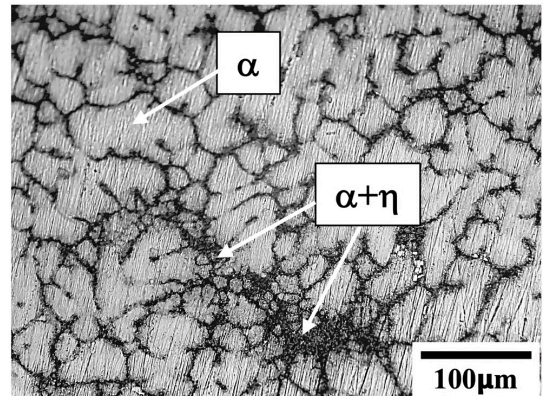
Casting method	Mechanical properties			
	Tensile strength (MPa)	Yield strength (MPa)	Elongation (%)	Hardness (HB) (kg <sup>2</sup> /mm <sup>2</sup> )
GDC	321	295	2.4	102
NRC	370	340	3	123

**Figure 6.** Transition from dendritic to semi-globular microstructure of ZA-27 alloy (a) Dendritic structure of GDC (b) Semi-globular structure of NRC.

transformation from the dendritic shape into a semi-globular structure consisting of a fine equiaxed  $\alpha$  phase bordered by eutectoid ( $\alpha$  and  $\eta$ ), as shown in Figure 6 and Figure 7. The microstructure changes in the NRC alloy resulted from, firstly, the utilization of inclined fluid director, which increases the formation of the nucleus on the mold wall due to increasing the contact area between the molten alloy and mold wall, which helps to gain a semi-solid slurry. Secondly, the isothermal holding step fuses the dendrite arm structure. Lastly, the quenching step presents the final solidification step, where the semi-solid alloy continues to solidify and produces the final semi-globular microstructure. The resulting microstructure of the non-dendritic shape contributes toward enhancing the mechanical properties of the ZA-27 alloy<sup>25,26</sup>. Table 2 illustrates the results of the tensile test and shows that strength was increased by about 15% in NRC in comparison to GDC. Furthermore, the elongation and hardness of NRC were increased by about 25% and 20%, respectively. These improvements in mechanical properties are attributed to the fact of the globular-shaped particles in the NRC sample may effectively reduce the stress concentration at the boundary between the  $\alpha$  phase and eutectoid ( $\alpha$  and  $\eta$ ) matrix under applied stresses. Therefore, the globular shape would improve the tensile strength as well as ductility in NRC alloy<sup>27,28</sup>.

### 3.2. Tribological behavior

Figure 8 shows the COF variation as a function of sliding speed. The experiment was carried out in dry and lubricated conditions at 20 N normal load. In dry condition, which is given in (Figure 8a), for both GDC and NRC alloys, the COF was increased slightly with sliding speed and showed nearly equal COF until the sliding speed reached 2 m/s. Then, the

**Figure 7.** Microstructure of ZA-27 alloy produced with NRC process.

COF for the GDC alloy was increased sharply when the sliding speed exceeds 2 m/s where the gap with the NRC alloy was significantly expanded. This sharp increment in the COF of GDC alloy after 2 m/s sliding speed is related to the pits, cavities, and deep grooves at the contact worn surface of the GDC alloy, resulting from the cutting and delamination of the material, which is clearly shown in (Figure 9a). The reason for this behavior was also discussed in Miloradović<sup>et al.7</sup>. On the other hand, the NRC alloy showed a stable and relatively low COF indicated by a smooth worn surface presented in Figure 9b. In particular, the COF behavior of NRC alloy can be attributed to the globular-shaped microstructure, which improves its wear resistance. Based on previous microstructure analysis, it is shown that the globular-shaped microstructure

reduces the stress concentration at the grain boundaries between the  $\alpha$  phase and eutectoid ( $\alpha$  and  $\eta$ ) matrix under applied load during the friction test and hence may reduce the crack tendency. This finding can also be seen in Figure 10, which presents a side view of a worn contact surface of NRC alloy at 20 N normal load and 3 m/s sliding speed. The contact worn surface appeared smoothly deformed with sliding direction and the semi-globular shape of grains changed to longitudinal without sign of cutting, delamination, and smears. Therefore, the rheo-processed sample exhibits greater wear resistance in severe wear conditions. This reason is consistent with the results discussed in Alhawari et al.<sup>29</sup>. For the sliding test with a lubricated condition, which is given in (Figure 8b), both GDC and NRC alloys showed lower and more stable friction level, and yet the NRC alloy had lower sliding friction

in comparison to the GDC alloy. This behavior reflects the significance of the microstructure used in wear resistance. However, in both conditions, the two casting types showed a steady-state friction behavior starting from 0.7 m/s up to 2 m/s sliding speed. Besides, for faster sliding speed, i.e., more than 2 m/s, the results showed the tribo-behavior stated transformation from adhesive to abrasive wear.

Figure 11 shows the dependence of COF on sliding time at a load of 20 N and 1.7 m/s for the ZA-27 GDC and NRC alloys. The test was performed under lubricated condition. Both alloys exhibit a steady state. Still, the NRC alloy recorded much lower sliding friction to about 67% lesser than the GDC alloy. This enhancement in wear resistance might be resulted from adhesive tribological behavior on the worn surface of the NRC alloy as shown in Figure 12. The improved mechanical properties of the NRC alloy compared to the GDC and the globular structure morphology of the NRC alloy versus dendritic in the GDC alloy had an impact on the tribological behavior. This finding agrees with the results presented by Miroslav et al.<sup>1</sup>.

The COF behavior variation relative to the normal load was also studied with the application of lubricant. Both GDC and NRC alloys showed a reduction in friction level when the load was increased with more steady and significantly reduced friction for the NRC alloys as indicated in Figure 13. During the process, increasing the normal load can lead to an increase in the effective stress over the elastic stress of asperities, which causes plastic deformation at their contact tip. The plastically deformed surface will fill the valley of the material in both the pin and the disc, and there is a chance of fracturing several asperities on both surfaces, resulting in fine debris and a smooth surface. This reason is inconsistent with Kumar and Dhiman<sup>30</sup> and Ghazi et al.<sup>31</sup>. Figure 14 shows the worn surfaces at 100N normal load for GDC and NRC alloys.

Figure 15 shows the wear resistance of GDC and NRC alloys based on weight loss as a function of normal load. The results show that weight loss increases as the normal forces increase. The highest weight loss was achieved in GDC alloys, which recorded remarkably higher values in comparison to the NRC across whole ranges of the normal forces that reflect the higher wear rate for the GDC alloy.

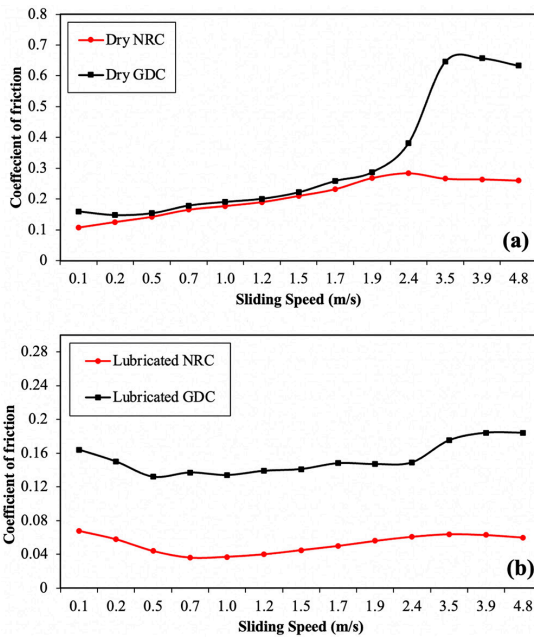


Figure 8. An illustration of friction coefficient variation with sliding speed (a) Dry condition (b) Lubricated condition.

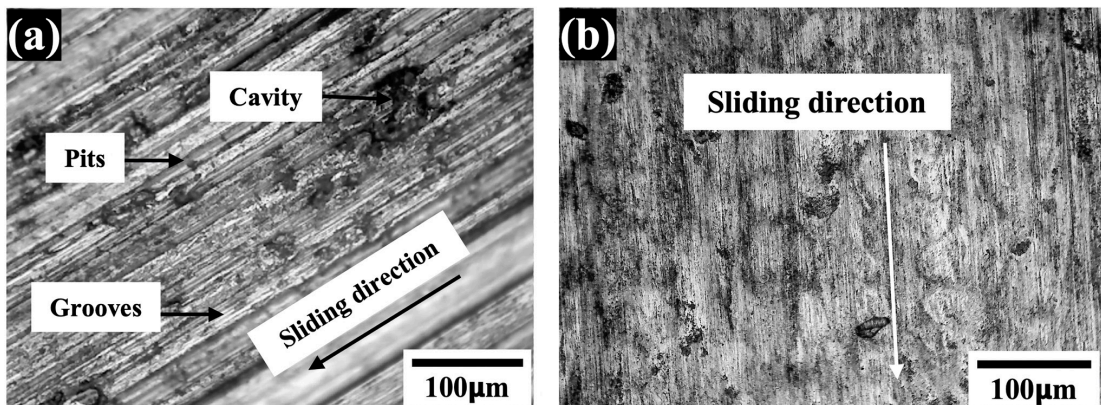


Figure 9. Optical micrograph of a worn surface (a) GDC alloy (b) NRC alloy, at 20 N normal load and 3 m/s sliding speed.

Figures 15 and 16 also illustrate that the wear rate and coefficient of wear respectively, in the GDC alloys is about 84% increment at 160 N normal load. The low wear resistance (high wear rate) of GDC alloy is owing to the delamination

and cutting wear, i.e., adhesive and abrasive wear, which results from the formation of debris at the contact surfaces of the alloy as shown in Figure 17, beside the crack propagation due to fatigue wear shown in Figure 18. The dark spots on

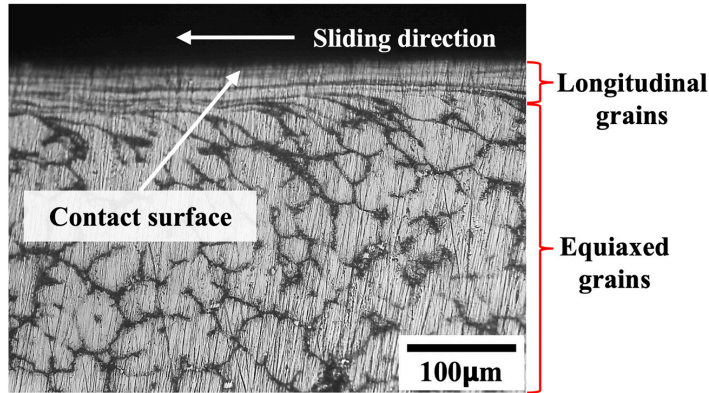


Figure 10. Side view showing a worn contact surface in NRC alloy at 20 N normal load and 3 m/s sliding speed.

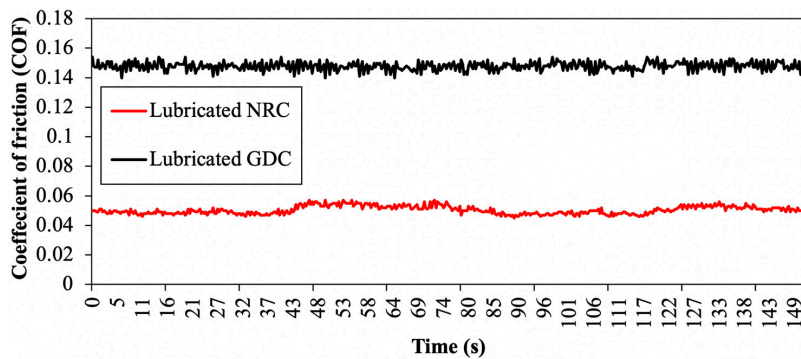


Figure 11. Friction coefficient behavior as a function of time for the GDC and NRC under lubricated condition at 1.7 m/s and 20 N normal load extracted for 150 sec of steady state.

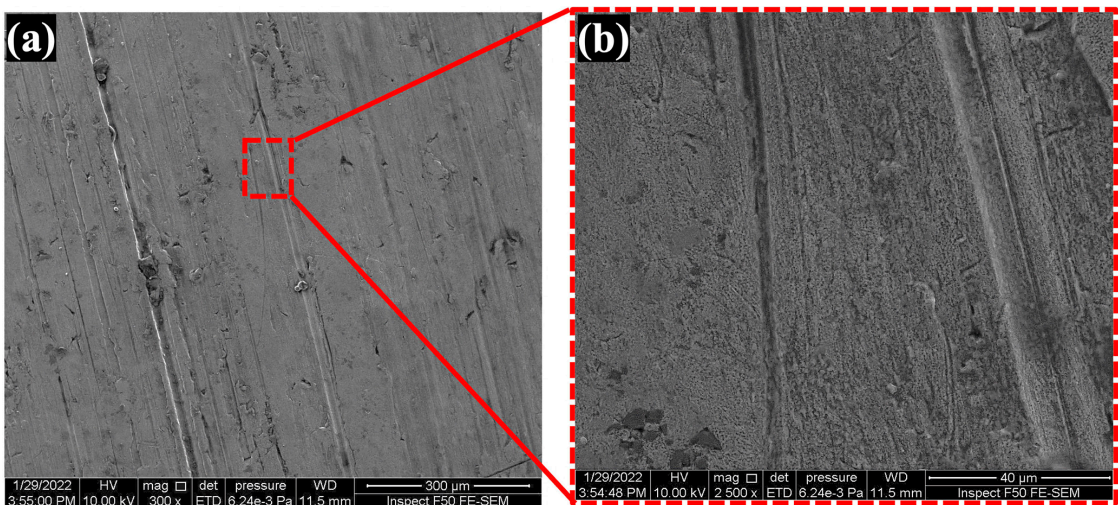


Figure 12. (a) Worn surface of NRC with adhesive wear (b) The NRC worn surface at higher magnification.

the worn surface are an indicator of a portion of high-cycle failure mode in the overall spectrum of wear mechanisms<sup>32</sup>. On the other hand, the NRC alloy showed a smooth surface and rebuilt debris as illustrated in Figure 19. These findings of NRC alloy can play a significant role in lowering the wear rate and enhancing the coefficient of wear Figure 16.

### 3.3. Correlation between microstructure and tribological behavior

To explain the NRC method's effect on the tribological behavior of Zn-Al alloys it is necessary to analyze the influence of the NRC method on the microstructure of the produced alloy. In general, Zn-Al alloys are a combination of the two solid solutions  $\alpha$  and  $\eta$  phases. Due to Al having a higher melting point compared to Zn, the  $\alpha$ -Al rich solid solution contributes to the strengthening and thermal stability of Zn-Al alloys. This phase, which has a face-centered cubic (FCC) crystal structure, also has a high work hardening capacity, which enhances the alloys' resistance to wear<sup>33,34</sup>. The c/a ratio of the hexagonal-close-packed (hcp) crystal structure of the  $\eta$ -Zn rich solid solution is greater than that

of the ideal close-packed hexagonal crystal system<sup>35</sup>. This property gives the micro component excellent smearing qualities as a solid lubricant<sup>35,36</sup>. The distribution and size of these micro-components determine the effects they have on the tribological behavior of the alloy.

GDC method revealed that the alloy had primary  $\alpha$  dendrites surrounded by a eutectoid  $\alpha+\eta$  mixture. This kind of dendritic structure is distinguished by the fact that the different micro-constituents are not distributed in a regulated manner (Figures 5 and 6a). In addition, residual stresses at the microscopic scale are caused by the varied thermal characteristics and mechanical properties of distinct phases<sup>37</sup>. By increasing the diffusion rate, the NRC method helped break up the nonequilibrium dendritic structure and increase the proportion of the  $\alpha+\eta$  combination in the final structure. Furthermore, the alloy's microstructure is refined, and its micro-constituents are distributed uniformly throughout. Increased elongation following NRC, caused by the transition from the metastable to the stable phase, is more evidence that this increase in uniformity reduces residual stresses. Characteristics of worn surfaces and wear mechanisms were investigated to help explain the observed tribological findings. The wear characteristics of both GDC and NRC alloys used in the tests are shown in Figures 9 and 14.

The worn surface of NRC alloys is generally smooth and includes shallow wear grooves as a consequence of light abrasive wear as presented with no signs of smearing as presented in Figure 12. In contrast, extensive abrasive and adhesive wear produces a much rougher surface in the GDC alloy (Figure 18), as shown by deep grooves, defects, and smeared material. Surface fatigue damages provide corroborative evidence that the phenomena of delamination lead to greater wear of the GDC alloy compared to the NRC one (Figure 18). Micro-scale residual stresses, caused by the non-uniform distribution of the different micro components, may explain the pronounced delamination wear of the GDC alloy (Figure 17). This GDC alloy wearing mechanism was seen during wear experiments under more

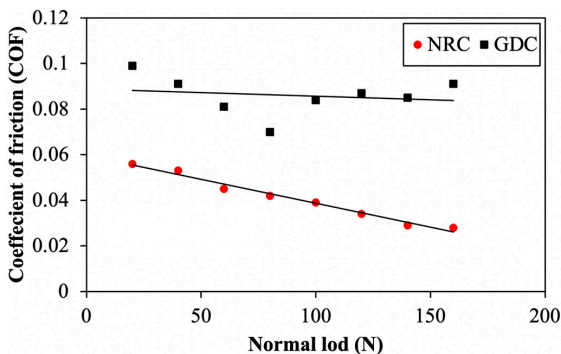


Figure 13. An illustration of friction coefficient as a function of normal load for the GDC and NRC under lubricated condition.

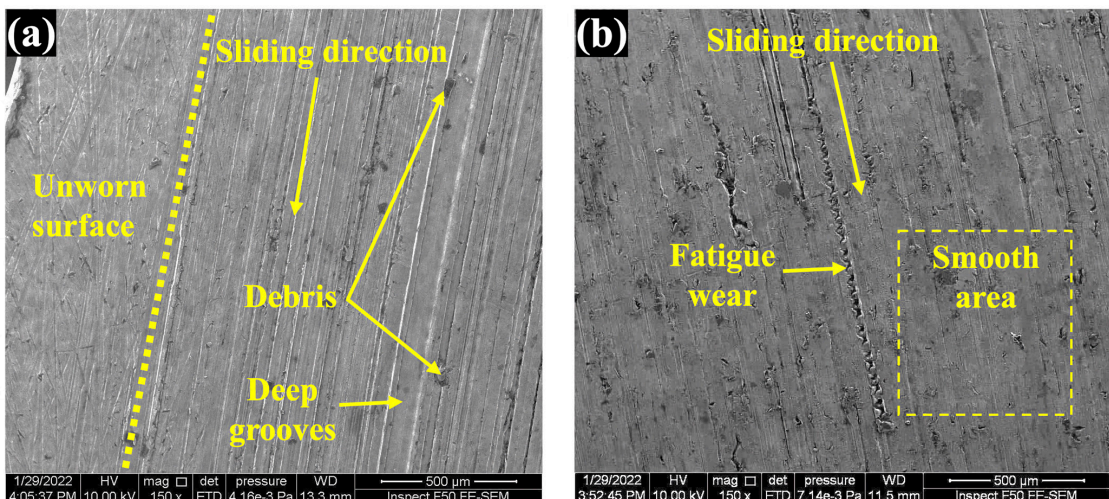


Figure 14. An illustration of a worn surface at 100N normal load for (a) GDC and (b) NRC.

severe conditions of load application. Features of wear surfaces match those predicted by the effects of applied load on the wear behavior of tested alloys (Figure 15). The GDC alloy line in the data plots has a much steeper slope than the NRC alloy line. The change in slope is most noticeable when the applied load is increased from about

40 to 75 N, and it becomes more noticeable when the load is increased to 100 N. The occurrence of delamination as a primary mechanism, which occurs in the region of higher applied loads, accounts for the observed difference between the wear rate increase with a load of GDC alloy and NRC alloys.

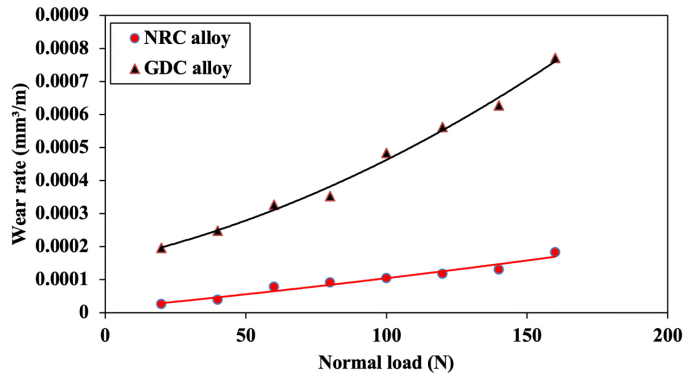


Figure 15. Wear rate as a function of normal load for the GDC and NRC alloys under lubricated conditions.

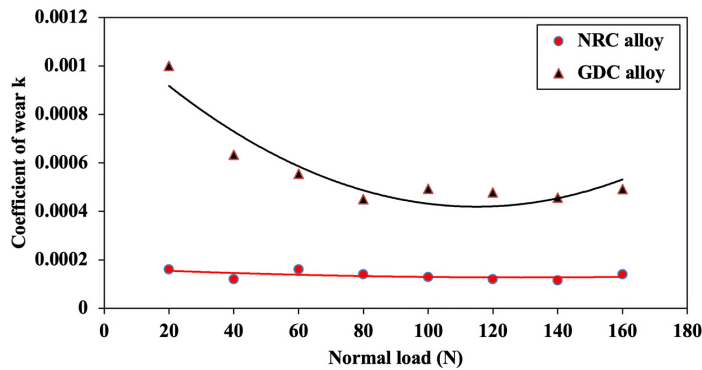


Figure 16. Coefficient of wear as a function of normal load for the GDC and NRC alloys under lubricated conditions.

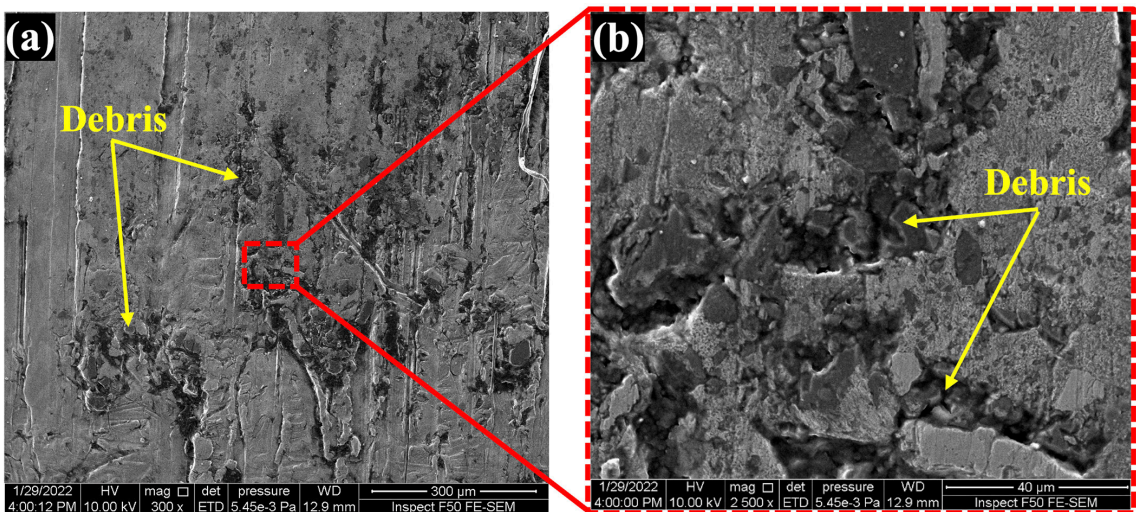


Figure 17. (a) Present of debris at worn GDC alloy surface (b) Debris in the GDC surface at high magnification.

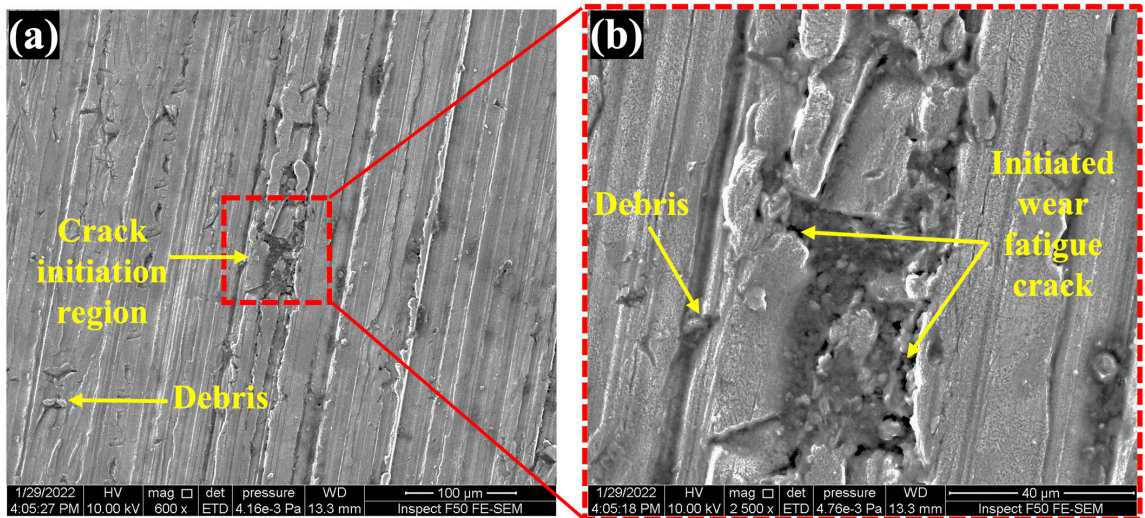


Figure 18. (a) Initiation of fatigue crack at worn GDC alloy surface (b) Initiation of fatigue crack at high magnification.

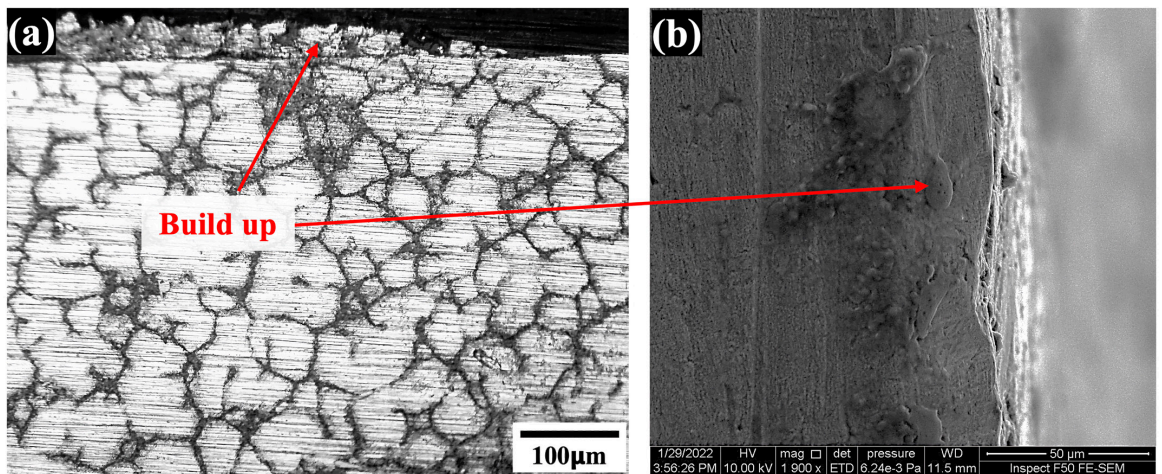


Figure 19. Build up at worn NRC alloy surface (a) Optical micrograph (side view) (b) Scanning electronic micrograph (top view).

#### 4. Conclusions

1. The microstructure of ZA-27 alloys produced with the GDC process is characterized by dendritic containing two phases ( $\alpha$  and  $\eta$ ), while the microstructure of the NRC alloys demonstrated a semi-globular structure consisting of fine equiaxed  $\alpha$  phase bordered by eutectoid ( $\alpha$  and  $\eta$ ).
2. The semi-globular structure of the NRC technique improved the mechanical properties of the ZA-27 alloy significantly in both tensile and hardness properties by about 15% and 20%, respectively. Also, the results showed that a 25% improvement in elongation is achieved.
3. The enhancement in mechanical properties of the NRC alloy improved the tribological behavior over GDC by reducing the COF to about 67% over the GDC alloy.

4. The wear rate with NRC was much lower than the rate of GDC with about 84% at 160 N normal load.
5. The worn surfaces of NRC alloys are characterized by smooth and shallow wear grooves. While the GDC alloy worn surfaces were rougher and had deeper grooves and damage. These achievements signify the importance of our research which can be very beneficial to both academic researchers and industries.

#### 5. References

1. Miroslav B, Vencel A, Mitrović S, Bobić I. Influence of T4 heat treatment on tribological behavior of Za27 alloy under lubricated sliding condition. *Tribol Lett.* 2009;36(2):125-34.
2. Murugaveni SP, Thyla PR. Assessing the performance of nano lubricant on zinc aluminium alloy. *Def Sci J.* 2019;69(4):396-401.
3. Mitrović S, Miloradović N, Babić M, Bobić I, Stojanović B, Džunić D. Wear behaviour of hybrid ZA27/SiC/graphite

- composites under dry sliding conditions. In: International Conference BULTRIB '12; 2012 Oct 18-20; Sofia. Proceedings. Sofia: Society of Bulgarian Tribologists; 2012. p. 142-7.
- Almomani MA, Hayajneh MT, Alelaumi SM. Applying Taguchi method to study the wear behaviour of ZA-27 alloy-based composites reinforced with SiC nanoparticles. *Int J Cast Met Res.* 2019;32(4):229-41.
  - Babic M, Stojanovic B, Dzunic D, Pantic M. Micro/nanoscale structural, mechanical and tribological characterization of ZA-27/SiC nanocomposites. *J Compos Mater.* 2020;54(16):2113-29.
  - Mitrović S, Babić M, Stojanović B, Miloradović N, Pantić M, Džunić D. Tribological potential of hybrid composites based on zinc and aluminium alloys reinforced with SiC and graphite particles. *Tribol Ind.* 2012;34(4):177-85.
  - Miloradović N, Vujanac R, Mitrović S, Miloradović D. Dry sliding wear performance of ZA27/SiC/Graphite composites. *Metals.* 2019;9(7):717.
  - Rajasekar M, Faizal UM, Sudhagar S, Vijayakumar P. Influence of heat treatment on tribological behavior of Al/ZrO<sub>2</sub>/fly ash hybrid composite. *Mater Today Proc.* 2021;45:774-9.
  - Bobić I, Babić M, Vencel A, Bobić B, Mitrović S. Artificial aging of thixocast ZA27 alloy and particulate ZA27/SiC p composites. *Int J Mater Res.* 2013;104(10):954-65.
  - Kumar NS. Mechanical and wear behavior of ZA-27/SiC/Gr hybrid metal matrix composites. *Mater Today Proc.* 2018;5(9):19969-75.
  - Fatile BO, Adewuyi BO, Owoyemi HT. Synthesis and characterization of ZA-27 alloy matrix composites reinforced with zinc oxide nanoparticles. *Eng Sci Technol Int J.* 2017;20(3):1147-54.
  - Güler O, Çuvalcı H, Gökdağ M, Çanakçı A, Çelebi M. Tribological behavior of ZA27/Al<sub>2</sub>O<sub>3</sub>/graphite hybrid nanocomposites. *Particul Sci Technol.* 2018;36(7):899-907.
  - Li G, Mao Y, Li Z, Wang L, Costa H. Tribological and corrosion properties of coatings produced by plasma electrolytic oxidation on the ZA27 alloy. *J Mater Eng Perform.* 2018;27(5):2298-305.
  - Yalçın ED, Çanakçı A, Erdemir F, Çuvalcı H, Karabacak AH. Enhancement of wear and corrosion resistance of ZA27/nanographene composites produced by powder metallurgy. *Arab J Sci Eng.* 2019;44(2):1437-45.
  - Ghazi A, Mejbel M. Tribological and mechanical performance of epoxy reinforced by fish scales powder. *J Compos Adv Mater.* 2022; 32(3):149-55.
  - LeHuy H, L'espérance G. Ageing characteristics of dendritic and non-dendritic (stir-cast) Zn-Al alloy (ZA-27). *J Mater Sci.* 1991;26(2):559-68.
  - Panpun C, Plookphol T, Janudom S. Creep of slurry squeeze-cast ZA-27 zinc alloy with different solid fractions at 140 °C. *Mater Sc Forum.* 2018;928:194-9.
  - Owoeye SS, Folorunso DO, Oji B, Borisade SG. Zinc-aluminum (ZA-27)-based metal matrix composites: a review article of synthesis, reinforcement, microstructural, mechanical, and corrosion characteristics. *Int J Adv Manuf Technol.* 2019;100(1-4):373-80.
  - Pola A, Montesano L, Gelfi M, Roberti R, La Vecchia GM. Aluminum segregation in ZA27 rheocast alloy. *Diffus Defect Data Solid State Data Pt B Solid State Phenom.* 2014;217-218:75-82.
  - Hu ZH, Wu GH, Xu J, Mo WF, Li YL, Liu WC et al. Dry wear behavior of rheo-casting Al-16Si-4Cu-0.5 Mg alloy. *Trans Nonferrous Met Soc China.* 2016;26(11):2818-29.
  - Kaufmann H, Potzinger R, Uggowitzer PJ. The relationship between processing and properties of new rheocast AZ 91 and AZ 71 magnesium parts. *Light Met Age.* 2001;59(1):56.
  - Abood AN, Habeb TS. Production of ZA-27 alloy by new rheocasting process. *J Zankoy Sulaimani Pt A.* 2008;11(1):89-99.
  - Azizan FM, Purwanto H, Mustafa MY. Effect of Sn addition on mechanical properties of zinc-based alloy. *Adv Mat Res.* 2012;576:378-81.
  - Bobić B, Vencel A, Ružić J, Bobić I, Damjanović Z. Microstructural and basic mechanical characteristics of ZA27 alloy-based nanocomposites synthesized by mechanical milling and compocasting. *J Compos Mater.* 2019;53(15):2033-46.
  - Kumar SD, Mandal A, Chakraborty M. Cooling slope casting process of semi-solid aluminum alloys: a review. *Int J Eng Res Technol.* 2014;3(7):269-83.
  - Abdelgnei MAH, Omar MZ, Ghazali MJ, Gebriil MA, Mohammed MN. The effect of the rheocast process on the microstructure and mechanical properties. *J Kejuruteraan.* 2019;31(2):317-26.
  - Zimpel I, Bartex SLT, Barcellos VK. Effects of stirring time and cooling rate on the rheocast microstructure and mechanical properties of magnesium alloy MRI 230D. *Mater Res.* 2021;24(3):e20200482.
  - Ming L, Yuan-Dong L, Wen-Long Y, Yu Z, Zong-Gang W. Effects of forming processes on microstructures and mechanical properties of A356 aluminum alloy prepared by self-inoculation method. *Mater Res.* 2019;22(3):e20180698.
  - Alhawari KS, Omar MZ, Ghazali MJ, Salleh MS, Mohammed MN. Dry sliding wear behaviour of thixoformed hypoeutectic Al-Si-Cu alloy with different amounts of magnesium. *Compos Interfaces.* 2016;23(6):519-31.
  - Kumar R, Dhiman S. A study of sliding wear behaviors of Al-7075 alloy and Al-7075 hybrid composite by response surface methodology analysis. *Mater Des.* 2013;50:351-9.
  - Ghazi AK, Taieh NK, Khudhur SK. Investigation of dry tribo-behavior of aluminum alloy AA6061/Al<sub>2</sub>O<sub>3</sub>/graphite composites synthesized by stir casting technique. *J Compos Adv Mater.* 2022;32(5):253-9.
  - Brykov MN, Akrytova TO, Osipov MJ, Petryshynets I, Puchy V, Efremenko VG et al. Abrasive wear of high-carbon low-alloyed austenite steel: microhardness, microstructure and X-ray characteristics of worn surface. *Materials.* 2021;14(20):6159.
  - Ilija B, Ninkovic R, Miroslav B. Structural and mechanical characteristics of composites with base matrix of RAR27 alloy reinforced with Al<sub>2</sub>O<sub>3</sub> and SiC particles. *Tribol Ind.* 2004;26(3-4):27.
  - Archard J. Contact and rubbing of flat surfaces. *J Appl Phys.* 1953;24(8):981-8.
  - El-Khair MTA, Daoud A, Ismail A. Effect of different Al contents on the microstructure, tensile and wear properties of Zn-based alloy. *Mater Lett.* 2004;58(11):1754-60.
  - Murphy S, Savaskan T. Comparative wear behaviour of Zn-Al-based alloys in an automotive engine application. *Wear.* 1984;98:151-61.
  - Prasad BK. Influence of heat treatment parameters on the lubricated sliding wear behaviour of a zinc-based alloy. *Wear.* 2004;257(11):1137-44.